Author(s): Kortelainen, Markus; Sun, Zhonghao; Hagen, Gaute; Nazarewicz, Witold; Papenbrock, Thomas; Reinhard, Paul-Gerhard

Title: Universal trend of charge radii of even-even Ca–Zn nuclei

Year: 2022

Version: Published version

Please cite the original version:

# Universal trend of charge radii of even-even Ca–Zn nuclei

Markus Kortelainen [1], Zhonghao Sun,[2,3] Gaute Hagen [3,2] Witold Nazarewicz [4]
Thomas Papenbrock [2,3] and Paul-Gerhard Reinhard [5]
[1]*Department of Physics, University of Jyväskylä, PB 35(YFL) FIN-40014 Jyväskylä, Finland*
[2]*Department of Physics and Astronomy, University of Tennessee, Knoxville, Tennessee 37996, USA*
[3]*Physics Division, Oak Ridge National Laboratory, Oak Ridge, Tennessee 37831, USA*
[4]*Department of Physics and Astronomy, FRIB Laboratory, Michigan State University, East Lansing, Michigan 48824, USA*
[5]*Institut für Theoretische Physik, Universität Erlangen, Erlangen, Germany*

Radii of nuclear charge distributions carry information about the strong and electromagnetic forces acting inside the atomic nucleus. Whereas the global behavior of nuclear charge radii is governed by the bulk properties of nuclear matter, their local trends are affected by quantum motion of proton and neutron nuclear constituents. The measured differential charge radii $\delta\langle r_c^2\rangle$ between neutron numbers $N = 28$ and $N = 40$ exhibit a universal pattern as a function of $n = N$–28 that is independent of the atomic number. Here we analyze this remarkable behavior in even-even nuclei from calcium to zinc using two state-of-the-art theories based on quantified nuclear interactions: the *ab initio* coupled cluster theory and nuclear density functional theory. Both theories reproduce the smooth rise of differential charge radii and their weak dependence on the atomic number. By considering a large set of isotopic chains, we show that this trend can be captured by just two parameters: the slope and curvature of $\delta\langle r_c^2\rangle(n)$. We demonstrate that these parameters show appreciable model dependence, and the statistical analysis indicates that they are not correlated with any single model property, i.e., they are impacted by both bulk nuclear properties as well as shell structure.

*Introduction.* High-precision measurements of nuclear charge radii offer unique information on the structure of atomic nuclei and fundamental symmetries of nature [1,2]. In particular, the precise data on variations of charge radii with proton and neutron numbers shed light on elusive aspects of nuclear behavior, such as superfluidity [3–6], shell structure [7,8], and correlations [9,10].

A case in point is the calcium isotopic chain in which the charge radii show an archlike behavior with pronounced odd-even staggering between the neutron magic numbers $N = 20$ and $N = 28$ with the charge radius of $^{48}$Ca very close to the value in $^{40}$Ca [11], followed by a steep rise resulting in unexpectedly large charge radii of neutron-rich isotopes [12]. Several structural effects contribute to this intricate pattern: smooth scaling of nuclear radii with the nuclear mass number as $A^{1/3}$, configuration mixing [13], the zero-point motion associated with surface vibrations [14], nucleonic pairing [15] in the presence of particle continuum [5], as well as nucleonic charge form factors and relativistic corrections [16]. In particular, the spin-orbit correction to nuclear charge density results in pronounced shell effects attributed to the population of spin-unsaturated single-particle orbits [16,17] that helps explaining the anomalous reduction in the charge radius in $^{48}$Ca.

The recent paper [7] showed that measured differential charge radii exhibit an element-independent steep increase beyond neutron number $N = 28$ from potassium ($Z = 19$) to

iron ($Z = 26$). The main aim of the present Letter is to address this puzzling behavior in even-even nuclei with atomic numbers $20 \leqslant Z \leqslant 30$ and $N \leqslant 40$. Experimentally, these nuclei exhibit a variety of structures, ranging from patterns characteristic of spherical nuclei in the vicinity of the nuclear magic numbers (here $N, Z = 20$ or $N, Z = 28$) to collective behavior attributed to well-deformed open-shell systems as, e.g., $^{60}$Fe. In these ranges of particle numbers, protons and neutrons move predominantly in the $1p0f$ shell-model orbitals, which, above $N = 28$, form a single pseudo-SU(3) shell [18,19] whose orbits have very similar radial behavior [20].

From a phenomenological perspective, local variations in charge radii are often attributed to core polarization effects due to valence nucleons [21] resulting in nuclear deformations [22]. Excellent insights were obtained by the seniority-model approach to nuclear radii [23,24], which is expected to work particularly well in the upper $1p0f$ shell because of the aforementioned pseudo-SU(3) symmetry. Moreover, because of the presence of nucleonic pairing, the variation of $\delta\langle r_c^2\rangle$ with particle numbers is expected to be smooth in even-even nuclei.

In the generalized seniority picture, for a given semimagic isotopic chain, the attractive interaction between the core nucleons and valence neutrons leads to a simple parabolic pattern of differential radii in even-$N$ isotopes [23,24],

$$\delta\langle r_c^2\rangle^{A_{\rm m}, A_{\rm m}+n} = an + bn^2, \tag{1}$$

where $n$ is defined as the number of neutrons above the shell closure at $N = N_m$ in the magic nucleus $A_m$, and $a$ and $b$ are constants. Experimentally, such a regular behavior has been seen in a number of even-even isotopes in the $0f_{7/2}$ region above $N_m = 20$ and is not limited to semimagic systems [25,26] For instance, for the calcium chain, assuming identical charge radii of $^{40}$Ca and $^{48}$Ca, Eq. (1) yields an archlike trend,

$$\delta \langle r_c^2 \rangle^{40,40+n} = \frac{n(8-n)}{16} \delta \langle r_c^2 \rangle^{40,44}. \qquad (2)$$

Considering the nuclei with $N > 28$, the generalized seniority scheme predicts that differential radii should behave according to Eq. (1) with $N_m = 28$. Below we show that charge radii predicted with nuclear energy density functionals (EDFs) and interactions from effective field theory (EFT) follow the pattern predicted by this simple model.

*Theoretical methods.* To understand the observed trends, we carried out a theoretical analysis using models that are capable of describing deformed nuclei. The first approach is the *ab initio* coupled cluster (CC) theory [27] that allows for systematically improvable calculations based on realistic Hamiltonians with nucleon-nucleon and three-nucleon potentials. The second approach is based on nuclear density functional theory (DFT) [28].

The comparison between *ab initio* and DFT results for the root-mean-square (rms) charge radii $\sqrt{\langle r_c^2 \rangle}$ and differential charge radii $\delta \langle r_c^2 \rangle^{A,A'} \equiv \langle r_c^2 \rangle^{A'} - \langle r_c^2 \rangle^A$, closely related to isotope shifts, has been presented in several recent papers [6,7,10,29]. In general, the energy-functional-based approach provides a more accurate description of nuclear global properties, including the total charge radii, whereas the local variations, e.g., differential radii, are better captured by Hamiltonian-based methods.

In our CC calculations, we employed the recently developed two- and three-nucleon $\Delta$NNLO$_{GO}$ interaction [30] with a cutoff of 394 MeV. This interaction from chiral EFT is based on pion exchange, short-ranged contacts, and, in contrast to many potentials derived within the framework of chiral effective field theory [31,32], the $\Delta$NNLO$_{GO}$ interaction also includes the effects of $\Delta$-resonance degrees of freedom [33–36]. The resulting potential yields an accurate description of bulk properties in finite nuclei and the saturation point and symmetry energy of nuclear matter [30].

We performed single-reference CC calculations in the singles and doubles (CCSD) approximation [37,38] using a natural-orbital basis computed from an axially symmetric parity conserving Hartree-Fock (HF) state [39] in a model space consisting of 15 harmonic oscillator shells ($N_{max} = 14$). This approach extends the previous computations of charge radii [29] to open-shell nuclei and allows us to describe deformed nuclei. Correlations beyond the mean field are captured by the ensuing CC computations. Our approach precludes the inclusion of effects from triaxial shapes (which are not expected to be significant in the nuclei we computed). We also note that the restoration of rotational invariance, i.e., the projection onto good total angular momentum, remains a challenge that we do not address in this Letter. The effects of the lacking symmetry restoration on the ground-state energy can be estimated from the projection of the HF energy [39].

TABLE I. Convergence of the CCSD ground-state binding energy ($E$) and charge radii ($R_{ch}$) in the natural-orbital basis for the nucleus $^{64}$Zn. The full space has $N_{max} = 14$, and truncated model spaces have dimensions equal to oscillator spaces with $N_{max}^{nat} = 6, 8, 10, 12$. See the text for the theoretical uncertainties.

| | $\hbar\omega = 12$ MeV | | $\hbar\omega = 16$ MeV | |
|---|---|---|---|---|
| $N_{max}^{nat}$ | $E$ (MeV) | $R_{ch}$ (fm) | $E$ (MeV) | $R_{ch}$ (fm) |
| 6 | −473.731 | 3.857 | −474.445 | 3.848 |
| 8 | −513.502 | 3.882 | −515.685 | 3.869 |
| 10 | −520.787 | 3.896 | −523.355 | 3.882 |
| 12 | −521.746 | 3.900 | −524.384 | 3.886 |

The HF density matrix is initialized by filling the last occupied single-particle orbits from low to high values of $|j_z|$, which yields a prolate deformed nucleus. After the HF equations are solved we compute a more accurate density matrix using second-order many-body perturbation theory [40] and obtain the natural orbital basis by diagonalizing the density matrix. Following Ref. [41] the normal-ordered Hamiltonian in the two-body approximation [42,43] is then truncated to a smaller model space (consisting of as many single-particle states as a harmonic-oscillator space with $N_{max}^{nat} = 12$) according to the occupation numbers of the natural orbitals with respect to the Fermi level. Table I shows the CCSD ground-state energy and the charge radius of $^{64}$Zn in model spaces with oscillator spacings of $\hbar\omega = 12$ and $\hbar\omega = 16$ MeV. We see that both the charge radius and the ground-state energy converge rapidly in the natural-orbital basis, and $N_{max}^{nat} = 12$ is sufficient for a converged result within 1 MeV. The results presented in this Letter are based on the oscillator spacing $\hbar\omega = 16$ MeV and $N_{max}^{nat} = 12$. The CCSD approximation omits triples excitations. Those increase the correlation energy by about 12% [39] and charge radii by less than 1% [44,45].

Figure 1 shows the ground-state energies of nuclei computed in this Letter in the CCSD approximation. For natural orbitals, the estimated triples correction is about 12% of the
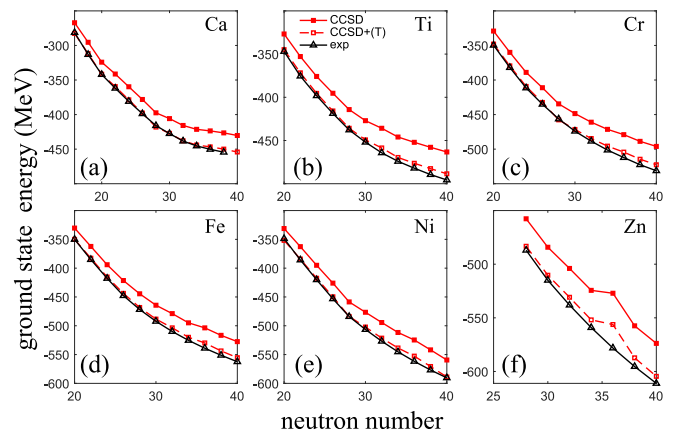


FIG. 1. Ground-state energies of nuclei computed in this Letter using the CCSD approximation (a)–(f). Also shown are CCSDs with estimated triples correction of 12% of the correlation energy and compared to data.

correlation energy. The nucleus $^{66}$Zn is an outlier and this might indicate that an axially symmetric prolate deformed reference state is not most adequate here.

In the calculation of rms charge radii from the CC proton-point radii, we took the nucleonic charge radii $\langle r_p^2 \rangle = 0.709$ and $\langle r_n^2 \rangle = -0.106$ fm$^2$ [46], and the Darwin-Foldy term $\langle r_{DF}^2 \rangle = 0.033$ fm$^2$. We also included the spin-orbit correction calculated within CC theory [29]. We have estimated that our *ab initio* CC results for charge radii carry $\pm 2\%$ uncertainty due to model-space and cluster-operator truncations [39].

Our DFT calculations were carried out using two different EDFs: the Skyrme parametrization SV-min [47] and the Fayans functional parametrization Fy($\Delta r$, HFB) [5,15]. Both functionals were optimized to the same large set of experimental observables from Ref. [47]. In addition, the Fy($\Delta r$, HFB) included differential radii of Ca isotopes. Its extended pairing functional turned out to be essential for reproducing charge radii in the Ca isotopic chain [5] and the kinks in charge radii at magic numbers [4].

The DFT calculations were performed with the SKYAX [48] and HFBTHO [49] solvers allowing for deformed solutions. For each nucleus, deformation energy minimum was located. All calculations with HFBTHO used oscillator basis functions up to $N_{sh} = 20$. Pairing with SKYAX was performed with a soft cutoff in single-particle space with a Woods-Saxon profile [50] reaching 15 MeV above the Fermi level with a smoothing with of 1.5 MeV. Results for spherical nuclei have been counterchecked with the spherical DFT solver, which was used for the calibration of the both functionals. Because of different descriptions of the continuum space, in HFBTHO pairing was renormalized to the results of spherical Fayans code.

DFT parametrizations being calibrated to empirical data carry statistical uncertainties from the calibration strategy, coined statistical errors. They can be estimated using the standard linear regression technique based on least squares [51]. Another source of error stems from limitations of the mean-field description. The largest systematic effects come from collective ground-state correlations associated with large amplitude collective motion (center-of-mass motion, rotations of deformed nuclei, and soft quadrupole vibrations). These correlations cannot be incorporated into a smooth density functional [52]. They were avoided in the fits of the functionals by including only nuclei which have negligible quadrupole correlations [47]. Here we are looking at nuclei outside that safe selection. To this end, we have computed the effect of collective ground-state correlations from low-lying $2^+$ states on charge radii [53]. The results are shown in Fig. 2. We take that as an estimate for the systematic error of the mean-field approximation. The DFT error bands for charge radii shown in the following represent statistical and systematic uncertainties.

The charge radii from DFT calculations were obtained as in Ref. [17] by folding the point charge distribution with the intrinsic nucleon form factors. In this way, the contributions from nucleonic charge form factors and relativistic corrections are automatically included.

*Results for charge radii.* The results of our CC and DFT calculations for the rms charge radii for even-even isotopic chains between calcium and zinc are shown in Fig. 3, in-
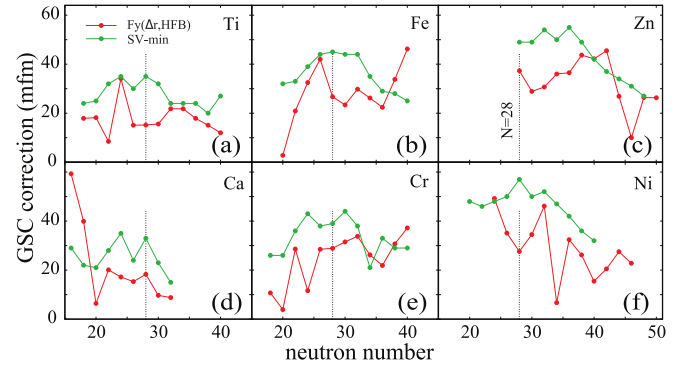


FIG. 2. Contribution to the charge radius from collective ground-state correlations caused by low-lying quadrupole states for the two DFT parametrizations used here.

cluding our estimates for theoretical uncertainties. The Fayans functional Fy($\Delta r$, HFB) provides a detailed description of experimental data for the Ca, Ti, and Cr isotopic chains. This is not surprising as Fy($\Delta r$, HFB) was optimized to the trends of charge radii in the selected Ca isotopes. For the light Ni and Zn nuclei, Fy($\Delta r$, HFB) systematically underestimates the charge radii. As discussed in Ref. [6], this is primarily related to the pairing in the $pf$-shell region: the pairing Fayans functional adjusted using data from the calcium region is too strong in heavier nuclei. The functional SV-min reproduces the charge radii data well, especially for the heavier isotopic chains. Its main deficiency is the underestimation of kinks in charge radii around magic gaps [4,15]. Generally, the employed $\Delta$NNLO$_{GO}$ interaction tends to predict slightly reduced radii compared to DFT results and experiment. The uncertainties depicted by the blue shaded area stem from finite model spaces and the cluster truncation. Those are strongly correlated, i.e., the entire blue line can shift horizontally within this band.

No pronounced irregularities in charge radii are seen at neutron numbers $N = 32, 34$, which have been predicted to be magic by some models. This conclusion is consistent with the
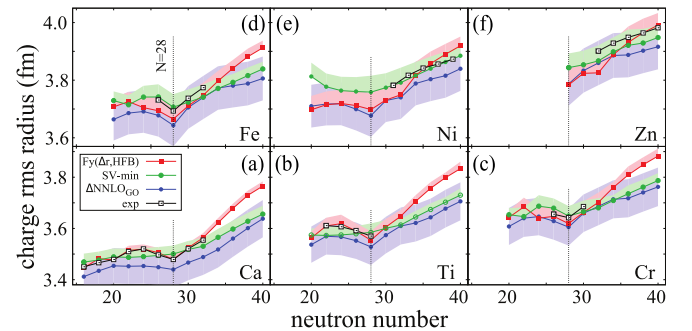


FIG. 3. Charge rms radii along the isotopic chains of (a) Ca, (b) Ti, (c) Cr, (d) Fe, (e) Ni, and (f) Zn. Results of CC and DFT calculations are compared to experimental data. The error bars for the DFT calculations are shown as red and green shaded areas, and the error bands for the CC calculations are shown as the blue shaded area. Experimental data were taken from Refs. [5,12] (Ca), [54] (Ti), [55] (Fe), [10,45] (Ni), [56] (Zn), and Ref. [57].
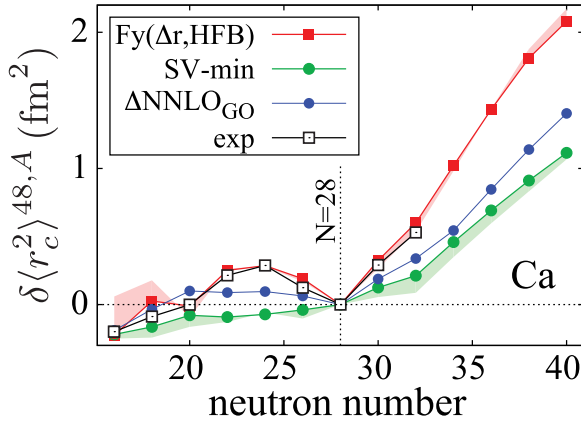
FIG. 4. Differential radii of the Ca isotopes. Theoretical uncertainties for CC calculations are discussed in the text.
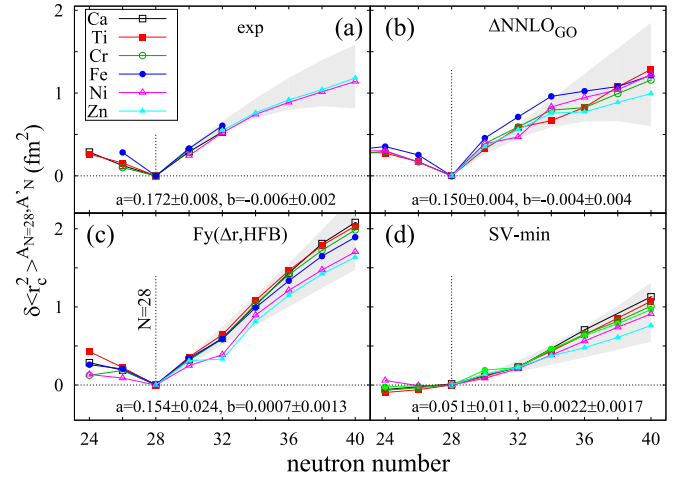


FIG. 5. (a) Experimental and (b)–(d) theoretical differential radii for the even-even Ca–Zn isotopic chains relative to the value of $\langle r_c^2 \rangle$ at $N = 28$. Theoretical error bars have been omitted. The values of $a$ and $b$ coefficients of Eq. (1) (in fm$^2$) obtained by a quadratic fit to $Z$-averaged differential radii for $N > 28$ are shown together with corresponding uncertainties (marked by a gray shading).

findings of Ref. [7], which studied this effect in the potassium isotopes.

As discussed earlier, the Ca chain represents the particular challenge for nuclear theory. This is illustrated in Fig. 4, which compares our predictions for the differential radii of the Ca isotopes with experiment. As expected, the local arch-like behavior between $^{40}$Ca and $^{48}$Ca, and a steep increase above $N = 28$ are both well reproduced by Fy($\Delta r$, HFB), which has been constrained by experimental values $\delta\langle r_c^2 \rangle^{40,48}$, $\delta\langle r_c^2 \rangle^{44,48}$, and $\delta\langle r_c^2 \rangle^{48,52}$, cf. also Eq. (2). The model SV-min yields a rather smooth monotonic increase in $\delta\langle r_c^2 \rangle^{48,A}$ with the neutron number. The results of $\Delta$NNLO$_{GO}$ fall in between. Because of strong correlations, the uncertainties of $\delta\langle r_c^2 \rangle^{48,A}$ well below 0.1 fm$^2$, see Ref. [39]. As indicated by Eq. (2) the value of the charge radius of the neutron open-shell nucleus $^{44}$Ca is important for understanding the trend in the Ca radii in the $0f_{7/2}$ region. Here, we note that the properties of $^{44}$Ca are strongly impacted by neutron pairing and that the specific pairing interaction of Fy($\Delta r$, HFB) has been crucial for describing the experimental trend. All three models predict an increase in the charge radius for $N > 28$. The rate of this increase is, however, model dependent.

Our main result is presented in Fig. 5, which shows $\delta\langle r_c^2 \rangle$ by comparing all isotopic chains in the same panel. As noted in Ref. [7], the measured charge radii beyond $N = 28$ exhibit a common increasing trend that is irrespective of the atomic number. This remarkable property is also present in our calculations: The predicted differential radii primarily depend on one quantity only: the number $n = N - 28$ of valence neutrons outside the $N = 28$ gap. However, the predicted values of $\delta\langle r_c^2 \rangle$ exhibit model-dependent patterns as a function of $n$.

The degree of $Z$ independence seen in experimental data is quite astonishing. It would be very interesting to see whether the experimental extension of the current limits of charge radii data for neutron-rich Ti, Cr, and Fe isotopes will confirm the pattern seen in Fig. 5. Due to the limited data supply at the experimental side and remaining errors at the theoretical side, the isotopic spread seen in theoretical results is greater than in experiment. Still, considering the scale of the deviations, the degree of isotopic consistency is quite good: the predicted model trends in $\delta\langle r_c^2 \rangle$ represent excellent benchmarks

for theory. A similar $Z$-independent pattern of $\delta\langle r_c^2 \rangle$ above $N = 28$ has recently been obtained in the Green's function approach [58] for $Z = 20, 22, 24$ and $N \leqslant 36$ with the interaction NNLO$_{sat}$. Below we compare their results to ours.

In order to quantify the $n$ dependence, we fitted the $Z$-averaged values of $\delta\langle r_c^2 \rangle$ to the parabolic expression (1). The resulting $a$ and $b$ coefficients are shown in Fig. 5 for experimental data and for each model. One sees that the $(a, b)$ values describing experimental differential charge radii are very close to those obtained in $\Delta$NNLO$_{GO}$: In both cases the pattern of charge radii is described by a parabola which is concave down. This result confirms the earlier observation that the local trends in charge radii in the $pf$ nuclei are well described by *ab initio* theory with chiral EFT interactions [6,7]. We note that our analysis of the Green's function results from Ref. [58], yields $a = 0.084 \pm 0.006$ fm$^2$, and $b = 0.003 \pm 0.001$ fm$^2$, i.e., their slope parameter is well below experimental and CC + $\Delta$NNLO$_{GO}$ values. The uncertainties on $a$ and $b$ indicate their variance over the ensemble. Their evaluation included the model uncertainties for SV-min and Fy($\Delta r$, HFB) but not for experiment where errors are too small to perform a visible effect. The statistical linear regression errors on $\Delta$NNLO$_{GO}$ predictions due to parameter calibration cannot be estimated at present. As mentioned above, the systematic truncation errors of CC calculations are highly correlated [39], and the associated uncertainties on differential radii can be practically neglected.

For Fy($\Delta r$, HFB), the average curvature coefficient $b$ is very close to zero. For SV-min, on the other hand $b$ is positive, i.e., the resulting pattern is concave up. To see whether the parameters $(a, b)$ contain information about specific model properties, we carried out a statistical least-squares regression study following the methodology described in Ref. [59]. This analysis requires the control of all model parameters simultaneously.
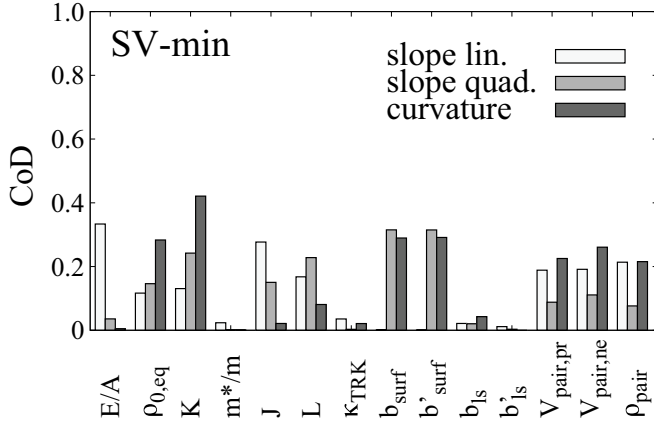
FIG. 6. Coefficients of determination between the parameters of SV-min and the slope and curvature coefficients of Eq. (1) fitted to the Z-averaged values of $\delta \langle r_c^2 \rangle$ of Fig. 5 with $28 \leqslant N \leqslant 40$.

The EDF parameters, characterizing its bulk properties, can be conveniently expressed through properties of symmetric nuclear matter; those are as follows: the equilibrium density $\rho_0$, the energy per nucleon at equilibrium $E/A$, the incompressibility $K$, the effective mass $m^*/m$ characterizing the dynamical isoscalar response, the symmetry energy $J$ and its slope $L$, and the Thomas-Reiche-Kuhn sum-rule enhancement $\kappa$ characterizing the dynamical isovector response, see Ref. [47] for definitions. In addition, we consider two parameters characterizing surface properties ($b_{\text{surf}}$ and $b'_{\text{surf}}$), two parameters characterizing spin-orbit terms ($b_{\text{ls}}$ and $b'_{\text{ls}}$), and three pairing parameters ($V_{\text{pair,pr}}$, $V_{\text{pair,ne}}$, and $\rho_{\text{pair}}$).

Figure 6 displays the results of our statistical analysis in terms of the coefficients of determination between the slope and curvature coefficients of Eq. (1) fitted to the Z-averaged values of $\delta \langle r_c^2 \rangle$ of Fig. 5 with $N \geqslant 28$. The coefficients of determination is a square of the bivariate correlation coefficient; it contains information on how well one quantity is determined by another one.

We carried out two fits. In the first variant (slope lin.), we estimated the average slope assuming no curvature. In the second variant, we estimated both the slope $a$ (slope quad.)

and the curvature $b$. Our analysis indicates that $(a, b)$ values are not correlated with one single model parameter, i.e., they are "distributed observables," and they are impacted by both bulk nuclear properties and shell structure.

*Discussion.* In conclusion, the regular pattern of the measured differential radii of even-even Ca–Zn nuclei beyond neutron number $N = 28$ has been analyzed by means of CC and DFT calculations extended to the open-shell deformed nuclei. Whereas the absolute charge radii are more accurately described by nuclear DFT, the local trends are very well modeled by CC calculations. Both theories reproduce the smooth rise of charge radii and their weak dependence on the atomic number.

The important finding of this Letter is that experimental and theoretical charge radii for these nuclei can be well parameterized in terms of a parabolic function of the number $n$ of valence neutrons outside the $N = 28$ magic gap. In particular, CC calculations reproduce both the slope and the curvature parameters describing the experimental $\delta \langle r_c^2 \rangle (n)$ dependence. Admittedly, the quantitative agreement with observations requires the microscopic understanding of the expansion coefficients $a$ and $b$. To trace back the values of these parameters to properties of nuclear forces and many-body correlations remains a theoretical challenge for future investigations.

[1] I. Counts, J. Hur, D. P. L. Aude Craik, H. Jeon, C. Leung, J. C. Berengut, A. Geddes, A. Kawasaki, W. Jhe, and V. Vuletić, Evidence for Nonlinear Isotope Shift in Yb$^+$ Search for New Boson, Phys. Rev. Lett. **125**, 123002 (2020).

[2] J. C. Berengut, C. Delaunay, A. Geddes, and Y. Soreq, Generalized King linearity and new physics searches with isotope shifts, Phys. Rev. Research **2**, 043444 (2020).

[3] M. Hammen, W. Nörtershäuser, D. L. Balabanski, M. L. Bissell, K. Blaum, I. Budinčević, B. Cheal, K. T. Flanagan, N. Frömmgen, G. Georgiev, C. Geppert, M. Kowalska, K. Kreim, A. Krieger, W. Nazarewicz, R. Neugart, G. Neyens, J. Papuga, P.-G. Reinhard, M. M. Rajabali, S. Schmidt, and D. T. Yordanov From Calcium to Cadmium: Testing the Pairing

Functional through Charge Radii Measurements of $^{100-130}$Cd, Phys. Rev. Lett. **121**, 102501 (2018).

[4] C. Gorges, L. V. Rodríguez, D. L. Balabanski, M. L. Bissell, K. Blaum, B. Cheal, R. F. Garcia Ruiz, G. Georgiev, W. Gins, H. Heylen, A. Kanellakopoulos, S. Kaufmann, M. Kowalska, V. Lagaki, S. Lechner, B. Maaß, S. Malbrunot-Ettenauer, W. Nazarewicz, R. Neugart, G. Neyens *et al.*, Laser Spectroscopy of Neutron-Rich Tin Isotopes: A Discontinuity in Charge Radii Across the $N = 82$ Shell Closure, Phys. Rev. Lett. **122**, 192502 (2019).

[5] A. J. Miller, K. Minamisono, A. Klose, D. Garand, C. Kujawa, J. D. Lantis, Y. Liu, B. Maaß, P. F. Mantica, W. Nazarewicz, W. Nörtershäuser, S. V. Pineda, P. G. Reinhard, D. M. Rossi,

F. Sommer, C. Sumithrarachchi, A. Teigelhöfer, and J. Watkins, Proton superfluidity and charge radii in proton-rich calcium isotopes, Nat. Phys. **15**, 432 (2019).

[6] R. P. de Groote, J. Billowes, C. L. Binnersley, M. L. Bissell, T. E. Cocolios, T. Day Goodacre, G. J. Farooq-Smith, D. V. Fedorov, K. T. Flanagan, S. Franchoo, R. F. Garcia Ruiz, W. Gins, J. D. Holt, Á. Koszorús, K. M. Lynch, T. Miyagi, W. Nazarewicz, G. Neyens, P. G. Reinhard, S. Rothe *et al.*, Measurement and microscopic description of odd-even staggering of charge radii of exotic copper isotopes, Nat. Phys. **16**, 620 (2020).

[7] Á. Koszorús, X. F. Yang, W. G. Jiang, S. J. Novario, S. W. Bai, J. Billowes, C. L. Binnersley, M. L. Bissell, T. E. Cocolios, B. S. Cooper, R. P. de Groote, A. Ekström, K. T. Flanagan, C. Forssén, S. Franchoo, R. F. G. Ruiz, F. P. Gustafsson, G. Hagen, G. R. Jansen, A. Kanellakopoulos *et al.*, Charge radii of exotic potassium isotopes challenge nuclear theory and the magic character of $N = 32$, Nat. Phys. **17**, 439 (2021).

[8] M. Reponen, R. P. de Groote, L. Al Ayoubi, O. Beliuskina, M. L. Bissell, P. Campbell, L. Cañete, B. Cheal, K. Chrysalidis, C. Delafosse, A. de Roubin, C. S. Devlin, T. Eronen, R. F. Garcia Ruiz, S. Geldhof, W. Gins, M. Hukkanen, P. Imgram, A. Kankainen, M. Kortelainen *et al.*, Evidence of a sudden increase in the nuclear size of proton-rich silver-96, Nat. Commun. **12**, 4596 (2021).

[9] D. T. Yordanov, L. V. Rodríguez, D. L. Balabanski, J. Bieroń, M. L. Bissell, K. Blaum, B. Cheal, J. Ekman, G. Gaigalas, R. F. Garcia Ruiz, G. Georgiev, W. Gins, M. R. Godefroid, C. Gorges, Z. Harman, H. Heylen, P. Jönsson, A. Kanellakopoulos, S. Kaufmann, C. H. Keitel *et al.*, Structural trends in atomic nuclei from laser spectroscopy of tin, Commun. Phys. **3**, 107 (2020).

[10] S. Malbrunot-Ettenauer, S. Kaufmann, S. Bacca, C. Barbieri, J. Billowes, M. L. Bissell, K. Blaum, B. Cheal, T. Duguet, R. F. Garcia Ruiz, W. Gins, C. Gorges, G. Hagen, H. Heylen, J. D. Holt, G. R. Jansen, A. Kanellakopoulos, M. Kortelainen, T. Miyagi, P. Navrátil *et al.*, Nuclear Charge Radii of the Nickel Isotopes $^{58-68,70}$Ni, Phys. Rev. Lett. **128**, 022502 (2021).

[11] H. J. Emrich, G. Fricke, G. Mallot, H. Miska, H.-G. Sieberling, J. Cavedon, B. Frois, and D. Goutte, Radial distribution of nucleons in the isotopes $^{48,40}$Ca, Nucl. Phys. A **396**, 401 (1983).

[12] R. F. Garcia Ruiz, M. L. Bissell, K. Blaum, A. Ekström, N. Frömmgen, G. Hagen, M. Hammen, K. Hebeler, J. D. Holt, G. R. Jansen *et al.*, Unexpectedly large charge radii of neutron-rich calcium isotopes, Nat. Phys. **12**, 594 (2016).

[13] E. Caurier, K. Langanke, G. Martínez-Pinedo, F. Nowacki, and P. Vogel, Shell model description of isotope shifts in calcium, Phys. Lett. B **522**, 240 (2001).

[14] F. Barranco and R. Broglia, Correlation between mean square radii and zero-point motions of the surface in the Ca isotopes, Phys. Lett. B **151**, 90 (1985).

[15] P.-G. Reinhard and W. Nazarewicz, Toward a global description of nuclear charge radii: Exploring the fayans energy density functional, Phys. Rev. C **95**, 064328 (2017).

[16] J. L. Friar and J. W. Negele, Theoretical and experimental determination of nuclear charge distributions, Adv. Nucl. Phys. **8**, 219 (1975).

[17] P.-G. Reinhard and W. Nazarewicz, Nuclear charge densities in spherical and deformed nuclei: Toward precise calculations of charge radii, Phys. Rev. C **103**, 054310 (2021).

[18] A. Arima, M. Harvey, and K. Shimizu, Pseudo ls coupling and pseudo Su$_3$ coupling schemes, Phys. Lett. B **30**, 517 (1969).

[19] R. D. Ratna Raju, J. P. Draayer, and K. T. Hecht, Search for a coupling scheme in heavy deformed nuclei: The pseudo SU(3) model, Nucl. Phys. A **202**, 433 (1973).

[20] D. Troltenier, W. Nazarewicz, Z. Szymański, and J. Draayer, On the validity of the pseudo-spin concept for axially symmetric deformed nuclei, Nucl. Phys. A **567**, 591 (1994).

[21] A. Bohr, The coupling of nuclear surface oscillations to the motion of individual nucleons, Dan. Mat. Fys. Medd. 26, 14 (1952).

[22] P. Brix and H. Kopfermann, Isotope shift studies of nuclei, Rev. Mod. Phys. **30**, 517 (1958).

[23] L. Zamick, Two body contribution to the effective radius operator, Ann. Phys. (NY) **66**, 784 (1971).

[24] I. Talmi, On the odd-even effect in the charge radii of isotopes, Nucl. Phys. A **423**, 189 (1984).

[25] M. Avgoulea, Y. P. Gangrsky, K. P. Marinova, S. G. Zemlyanoi, S. Fritzsche, D. Iablonskyi, C. Barbieri, E. C. Simpson, P. D. Stevenson, J. Billowes, P. Campbell, B. Cheal, B. Tordoff, M. L. Bissell, D. H. Forest, M. D. Gardner, G. Tungate, J. Huikari, A. Nieminen, H. Penttilä *et al.*, Nuclear charge radii and electromagnetic moments of radioactive scandium isotopes and isomers, J. Phys. G: Nucl. Part. Phys. **38**, 025104 (2011).

[26] H. D. Wohlfahrt, E. B. Shera, M. V. Hoehn, Y. Yamazaki, and R. M. Steffen, Nuclear charge distributions in $1f_{\frac{7}{2}}$-shell nuclei from muonic x-ray measurements, Phys. Rev. C **23**, 533 (1981).

[27] G. Hagen, T. Papenbrock, M. Hjorth-Jensen, and D. J. Dean, Coupled-cluster computations of atomic nuclei, Rep. Prog. Phys. **77**, 096302 (2014).

[28] M. Bender, P.-H. Heenen, and P.-G. Reinhard, Self-consistent mean-field models for nuclear structure, Rev. Mod. Phys. **75**, 121 (2003).

[29] G. Hagen, A. Ekström, C. Forssén, G. R. Jansen, W. Nazarewicz, T. Papenbrock, K. A. Wendt, S. Bacca, N. Barnea, B. Carlsson, C. Drischler, K. Hebeler, M. Hjorth-Jensen, M. Miorelli, G. Orlandini, A. Schwenk, and J. Simonis, Neutron and weak-charge distributions of the $^{48}$Ca nucleus, Nat. Phys. **12**, 186 (2015).

[30] W. G. Jiang, A. Ekström, C. Forssén, G. Hagen, G. R. Jansen, and T. Papenbrock, Accurate bulk properties of nuclei from $a = 2$ to $\infty$ from potentials with $\Delta$ isobars, Phys. Rev. C **102**, 054301 (2020).

[31] E. Epelbaum, H.-W. Hammer, and U.-G. Meißner, Modern theory of nuclear forces, Rev. Mod. Phys. **81**, 1773 (2009).

[32] R. Machleidt and D. R. Entem, Chiral effective field theory and nuclear forces, Phys. Rep. **503**, 1 (2011).

[33] N. Kaiser, S. Gerstendörfer, and W. Weise, Peripheral nn-scattering: Role of delta-excitation, correlated two-pion and vector meson exchange, Nucl. Phys. A **637**, 395 (1998).

[34] H. Krebs, E. Epelbaum, and U.-G. Meißner, Nuclear forces with $\Delta$ excitations up to next-to-next-to-leading order, part I: Peripheral nucleon-nucleon waves, Eur. Phys. J. A **32**, 127 (2007).

[35] E. Epelbaum, H. Krebs, and U.-G. Meißner, $\Delta$-excitations and the three-nucleon force, Nucl. Phys. A **806**, 65 (2008).

[36] M. Piarulli, L. Girlanda, R. Schiavilla, R. N. Pérez, J. E. Amaro, and E. R. Arriola, Minimally nonlocal nucleon-nucleon potentials with chiral two-pion exchange including $\Delta$ resonances, Phys. Rev. C **91**, 024003 (2015).

[37] H. Kümmel, K. H. Lührmann, and J. G. Zabolitzky, Many-fermion theory in expS- (or coupled cluster) form, Phys. Rep. **36**, 1 (1978).

[38] R. J. Bartlett and M. Musiał, Coupled-cluster theory in quantum chemistry, Rev. Mod. Phys. **79**, 291 (2007).

[39] S. J. Novario, G. Hagen, G. R. Jansen, and T. Papenbrock, Charge radii of exotic neon and magnesium isotopes, Phys. Rev. C **102**, 051303(R) (2020).

[40] A. Tichai, J. Müller, K. Vobig, and R. Roth, Natural orbitals for ab initio no-core shell model calculations, Phys. Rev. C **99**, 034321 (2019).

[41] J. Hoppe, A. Tichai, M. Heinz, K. Hebeler, and A. Schwenk, Natural orbitals for many-body expansion methods, Phys. Rev. C **103**, 014321 (2021).

[42] G. Hagen, T. Papenbrock, D. J. Dean, A. Schwenk, A. Nogga, M. Włoch, and P. Piecuch, Coupled-cluster theory for three-body hamiltonians, Phys. Rev. C **76**, 034302 (2007).

[43] R. Roth, S. Binder, K. Vobig, A. Calci, J. Langhammer, and P. Navrátil, Medium-Mass Nuclei with Normal-Ordered Chiral $nn + 3n$ Interactions, Phys. Rev. Lett. **109**, 052501 (2012).

[44] M. Miorelli, S. Bacca, G. Hagen, and T. Papenbrock, Computing the dipole polarizability of $^{48}$Ca with increased precision, Phys. Rev. C **98**, 014324 (2018).

[45] S. Kaufmann, J. Simonis, S. Bacca, J. Billowes, M. L. Bissell, K. Blaum, B. Cheal, R. F. G. Ruiz, W. Gins, C. Gorges, G. Hagen, H. Heylen, A. Kanellakopoulos, S. Malbrunot-Ettenauer, M. Miorelli, R. Neugart, G. Neyens, W. Nörtershäuser, R. Sánchez, S. Sailer, A. Schwenk, T. Ratajczyk, L. V. Rodríguez, L. Wehner, C. Wraith, L. Xie, Z. Y. Xu, X. F. Yang, and D. T. Yordanov, Charge Radius of the Short-Lived $^{68}$Ni and Correlation with the Dipole Polarizability, Phys. Rev. Lett. **124**, 132502 (2020).

[46] A. A. Filin, V. Baru, E. Epelbaum, H. Krebs, D. Möller, and P. Reinert, Extraction of the Neutron Charge Radius from A Precision Calculation of the Deuteron Structure Radius, Phys. Rev. Lett. **124**, 082501 (2020).

[47] P. Klüpfel, P.-G. Reinhard, T. J. Bürvenich, and J. A. Maruhn, Variations on a theme by skyrme: A systematic study of adjustments of model parameters, Phys. Rev. C **79**, 034310 (2009).

[48] P.-G. Reinhard, B. Schuetrumpf, and J. A. Maruhn, The axial Hartree-Fock + BCS Code SkyAx, Comput. Phys. Commun. **258**, 107603 (2021).

[49] M. V. Stoitsov, N. Schunck, M. Kortelainen, N. Michel, H. Nam, E. Olsen, J. Sarich, and S. Wild, Axially deformed solution of the Skyrme-Hartree-Fock-Bogoliubov equations using the transformed harmonic oscillator basis (II) HFBTHO v2.00d: A new version of the program, Comput. Phys. Commun. **184**, 1592 (2013).

[50] S. J. Krieger, P. Bonche, H. Flocard, P. Quentin, and M. S. Weiss, An improved pairing interaction for mean–field calculations using Skyrme potentials, Nucl. Phys. A **517**, 275 (1990).

[51] J. Dobaczewski, W. Nazarewicz, and P.-G. Reinhard, Error estimates of theoretical models: A guide, J. Phys. G: Nucl. Part. Phys. **41**, 074001 (2014).

[52] R. M. Dreizler and E. K. U. Gross, *Density Functional Theory: An Approach to the Quantum Many-Body Problem* (Springer-Verlag, Berlin, 1990).

[53] P. Klüpfel, J. Erler, P.-G. Reinhard, and J. A. Maruhn, Systematics of collective correlation energies from self-consistent mean-field calculations, Eur. Phys. J. A **37**, 343 (2008).

[54] Y. P. Gangrsky, K. P. Marinova, S. G. Zemlyanoi, I. D. Moore, J. Billowes, P. Campbell, K. T. Flanagan, D. H. Forest, J. A. R. Griffith, J. Huikari, R. Moore, A. Nieminen, H. Thayer, G. Tungate, and J. Äystö, Nuclear charge radii of neutron deficient titanium isotopes $^{44}$Ti and $^{45}$Ti, J. Phys. G: Nucl. Part. Phys. **30**, 1089 (2004).

[55] K. Minamisono, D. M. Rossi, R. Beerwerth, S. Fritzsche, D. Garand, A. Klose, Y. Liu, B. Maaß, P. F. Mantica, A. J. Miller, P. Müller, W. Nazarewicz, W. Nörtershäuser, E. Olsen, M. R. Pearson, P.-G. Reinhard, E. E. Saperstein, C. Sumithrarachchi, and S. V. Tolokonnikov, Charge Radii of Neutron Deficient $^{52,53}$Fe Produced by Projectile Fragmentation, Phys. Rev. Lett. **117**, 252501 (2016).

[56] L. Xie, X. Yang, C. Wraith, C. Babcock, J. Bieroń, J. Billowes, M. Bissell, K. Blaum, B. Cheal, L. Filippin, K. Flanagan, R. Garcia Ruiz, W. Gins, G. Gaigalas, M. Godefroid, C. Gorges, L. Grob, H. Heylen, P. Jönsson, S. Kaufmann *et al.*, Nuclear charge radii of $^{62-80}$Zn and their dependence on cross-shell proton excitations, Phys. Lett. B **797**, 134805 (2019).

[57] I. Angeli and K. P. Marinova, Table of experimental nuclear ground state charge radii: An update, At. Data Nucl. Data Tables **99**, 69 (2013).

[58] V. Somà, C. Barbieri, T. Duguet, and P. Navrátil, Moving away from singly-magic nuclei with Gorkov Green's function theory, Eur. Phys. J. A **57**, 135 (2021).

[59] B. Schuetrumpf, W. Nazarewicz, and P.-G. Reinhard, Central depression in nucleonic densities: Trend analysis in the nuclear density functional theory approach, Phys. Rev. C **96**, 024306 (2017).